Article

G Protein-Coupled Receptors Self-Assemble in Dynamics Simulations of Model Bilayers

Xavier Periole, Thomas Huber, Siewert-Jan Marrink, and Thomas P. Sakmar

J. Am. Chem. Soc., **2007**, 129 (33), 10126-10132• DOI: 10.1021/ja0706246 • Publication Date (Web): 21 July 2007

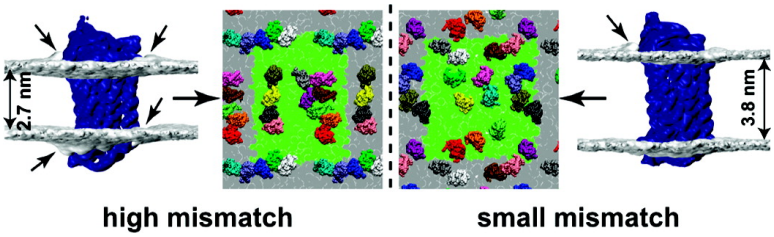

More About This Article

Additional resources and features associated with this article are available within the HTML version:

- Supporting Information
- Links to the 11 articles that cite this article, as of the time of this article download
- Access to high resolution figures
- Links to articles and content related to this article
- Copyright permission to reproduce figures and/or text from this article

View the Full Text HTML

J|A|C|S
ARTICLES
Published on Web 07/21/2007

G Protein-Coupled Receptors Self-Assemble in Dynamics Simulations of Model Bilayers

Xavier Periole,*,† Thomas Huber,*,‡ Siewert-Jan Marrink,† and Thomas P. Sakmar‡

Contribution from the Groningen Biomolecular Sciences and Biotechnology Institute, Department of Biophysical Chemistry, University of Groningen, Nijenborgh 4, 9747 AG Groningen, The Netherlands, and Laboratory of Biochemistry and Molecular Biology, The Rockefeller University, 1230 York Avenue, New York, New York 10021

Received January 28, 2007; E-mail: x.periole@rug.nl; hubert@rockefeller.edu

Abstract: Many integral membrane proteins assemble to form oligomeric structures in biological membranes. In particular, seven-transmembrane helical G protein-coupled receptors (GPCRs) appear to self-assemble constitutively in membranes, but the mechanism and physiological role of this assembly are unknown. We developed and employed coarse-grain molecular dynamics (CGMD) models to investigate the molecular basis of how the physicochemical properties of the phospholipid bilayer membrane affect self-assembly of visual rhodopsin, a prototypical GPCR. The CGMD method is a mesoscopic simulation technique in which groups of atoms are mapped to particles on the basis of a four-to-one rule. This systematic reduction of the degrees of freedom allows for computationally efficient calculation of the structure and dynamics of molecular assemblies for larger time and length scales than accessible to atomistic models, providing here an unprecedented view of spontaneous protein assembly in biomembranes. Systems with up to 16 rhodopsin molecules at a protein-to-lipid ratio of 1:100 were simulated for time scales of up to 8 μs. The results obtained for four different phospholipid environments showed that localized adaptation of the membrane bilayer to the presence of receptors is reproducibly most pronounced near transmembrane helices 2, 4, and 7. This local membrane deformation appears to be a key factor defining the rate, extent, and orientational preference of protein−protein association. The implications of our findings are discussed within a framework of a generalized mechanism of membrane protein self-assembly.

Introduction

The classical fluid mosaic model of cell membranes[1] describes a two-dimensional liquid-like solution of membrane proteins. In many cases, integral membrane proteins, including channels and receptors for transmembrane (TM) signaling, assemble into oligomeric structures during biogenesis or in response to ligand binding. In addition, self-assembly or self-organization of membrane proteins into dimers and higher-order structures seems to be involved in sorting and compartmentalization of membrane components.[2,3] In particular, 7-TM helical G protein-coupled receptors (GPCRs), such as the visual receptor rhodopsin, appear to self-assemble constitutively in membranes.[4−6] However, the mechanism and physiological role of this assembly are unknown. Moreover, at least in some cases, random interactions might have been mistaken for true dimerization.[7] In order to address the question of how lipid−protein interactions and continuum elastic membrane properties influence the monomer versus dimer stability or the oligomerization propensity of TM proteins, we attempt to establish a model system amenable to both experimental and theoretical approaches. Our long-term goal is a detailed thermodynamic picture of the self-assembly process of TM proteins together with a description of protein structural features that facilitate or counteract self-assembly. Understanding the interplay between specific lipid−protein interactions and continuum elastic membrane properties is thought to be one of the central challenges in biological chemistry.[8]

Hydrophobic mismatch, defined as the difference between the length of the hydrophobic part of a TM protein and the equilibrium hydrophobic bilayer thickness,[9,10] was shown to promote self-assembly of rhodopsin reconstituted in membrane bilayers.[11−14] Moreover, the effect of bilayer thickness on the acid−base equilibrium coupled to rhodopsin activation appeared to be directly correlated with changes in the oligomerization

† University of Groningen.
‡ Rockefeller University.

(1) Singer, S. J.; Nicolson, G. L. *Science* **1972**, *175*, 720−731.
(2) Vereb, G.; Szollosi, J.; Matko, J.; Nagy, P.; Farkas, T.; Vigh, L.; Matyus, L.; Waldmann, T. A.; Damjanovich, S. *Proc. Natl. Acad. Sci. U.S.A.* **2003**, *100*, 8053−8058.
(3) Engelman, D. M. *Nature* **2005**, *438*, 578−580.
(4) Fotiadis, D.; Liang, Y.; Filipek, S.; Saperstein, D. A.; Engel, A.; Palczewski, K. *Nature* **2003**, *421*, 127−128.
(5) Milligan, G. *Mol. Pharmacol.* **2004**, *66*, 1−7.
(6) Terrillon, S.; Bouvier, M. *EMBO Rep.* **2004**, *5*, 30−34.
(7) James, J. R.; Oliveira, M. I.; Carmo, A. M.; Iaboni, A.; Davis, S. J. *Nat. Methods* **2006**, *3*, 1001−1006.
(8) Zimmerberg, J.; Gawrisch, K. *Nat. Chem. Biol.* **2006**, *2*, 564−567.
(9) Killian, J. A. *Biochim. Biophys. Acta* **1998**, *1376*, 401−416.
(10) Lee, A. G. *Biochim. Biophys. Acta−Biomembr.* **2004**, *1666*, 62−87.
(11) Kusumi, A.; Hyde, J. S. *Biochemistry* **1982**, *21*, 5978−5983.
(12) Pearson, L. T.; Chan, S. I.; Lewis, B. A.; Engelman, D. M. *Biophys. J.* **1983**, *43*, 167−174.
(13) Ryba, N. J. P.; Marsh, D. *Biochemistry* **1992**, *31*, 7511−7518.
(14) Botelho, A. V.; Huber, T.; Sakmar, T. P.; Brown, M. F. *Biophys. J.* **2006**, *91*, 4464−4477.

10.1021/ja0706246 CCC: $37.00

state.[14] This rather unexpected finding was a key motivation to investigate the association mechanism in molecular detail. Although it has several unique features due to its role as a photoreceptor molecule, rhodopsin is a prototypical family A GPCR and has been employed extensively as a GPCR model system;[15,16] our findings may thus apply to other GPCRs.

The increasing number of available crystal structures of integral membrane proteins drives the quest for novel theoretical tools to study their behavior in native-like membrane assemblies.[17−19] In that regard, one technique that shows considerable promise is coarse-grain molecular dynamics (CGMD) simulations.[20−26] By reducing the degree of description of the system from atoms to chemical groups formed by 3−6 nonhydrogen atoms, this technique fulfils the required increase in system size and time scale as compared to a full atomistic approach, but conserves the physicochemical properties of the system, thus assuring the right balance of forces. This technique has been particularly successful in describing several mesoscopic phenomena involving membrane bilayers.[22,27,28] As shown here, the CGMD method allows researchers to study organization of membrane proteins in systems well beyond simple pairs of TM helices, thus closing the gap between lattice models[17] and atomistic simulations.[18]

Here we have extended this approach to the modeling of proteins in order to address the question of how the physicochemical properties of the membrane lipids might affect self-assembly of integral membrane proteins. In particular, we investigate the role of lipid diversity[8] in the self-assembly process of rhodopsin. First, simulations of rhodopsin as a monomer (Supporting Information, Movie 1) were used to characterize the response of both the protein and the bilayer to the presence of hydrophobic mismatch. Next, we carried out multi-copy rhodopsin simulations (16 proteins per unit cell; Supporting Information, Movies 2 and 3) at a protein-to-lipid ratio of 1:100 in the same bilayer environments. From an initial condition out-of-equilibrium, where the proteins were fully dispersed and ordered in the bilayer cell, we followed the relaxation of the system and analyzed the simulations with the aim of characterizing the mechanism by which rhodopsins progressively self-assemble into aggregates and ordered linear arrays. We found that localized adaptation of the membrane bilayer to the protein and surface complementarity are key factors defining the rate, extent, and orientational preference of protein−protein association. The results show rhodopsin association as a multi-stage mechanism, similar to recent models developed for globular proteins.[29−31]

Methods

Models. In our CG model,[22] small groups of atoms (3−6 heavy atoms) are united into single interaction centers. All particles interact through pairwise short-range Lennard-Jones and Coulomb potentials. The strength of the interaction depends on the chemical nature of the particles, which differ by their degree of hydrophilicity as reported by their partition coefficient between polar and apolar media. The latter is used as the basis for the parametrization of the model by means of the solvation free energy difference between water and butane. The procedure has been described in detail elsewhere for lipid molecules.[22]

The extension of the force field for the modeling of proteins was based on the same philosophy. Other groups have recently used similar approaches.[20,23] Each amino acid side chain was described by one or more interaction sites, according to their size, and their type was selected to reproduce as best as possible the solvation free energy difference of their side-chain analogue between polar and apolar media. The backbone was described by an apolar (N0) interaction site. Note that the association constants of side-chain beads mimicking salt-bridge and hydrophobic side-chain interactions were in complete agreement with atomistic simulations.

The model for rhodopsin was designed to reproduce the shape, surface polarity, and dynamics of the inactive rhodopsin as reported by the 1L9H crystal structure,[32] in which the two missing segments were built as previously described.[33] In that respect, the original conformation and orientation of the helices and loops were constrained by the addition of artificial bonds between backbone beads. The irregularities of the structure, for example, the helix kink, are included. The surface polarity was described by the CG model for proteins, and the dynamics reported in the manuscript agree well with experimental data.

Simulations. The molecular dynamics simulations were performed using the GROMACS program package[34−36] with the protocol developed for CGMD simulations.[22] The systems were simulated at constant temperature and pressure under periodic boundary conditions. A time step of 40 fs resulted in a numerically stable integration.

The simulation times reported in the manuscript are effective times. The CG dynamics are faster than the all-atom dynamics because the CG interactions are much smoother compared to atomistic interactions.[22] Based on comparison on diffusion constants in the CG model and in atomistic models, the effective time sampled using the CG is 3−6-fold larger. When interpreting the simulations results with the CG model, a conversion factor of 4 is used, which is effectively a speed-up factor in the diffusion dynamics of CG water compared to real water.[22]

Analysis and visualizations were performed using the GROMACS[34−36] and VMD[37] program packages and our own scripts and programs. Details of the models and simulation protocols are published as Supporting Information.

Results

We first analyzed the adaptation of the lipid−water interface to the hydrophobic surface of monomeric rhodopsin (one protein

(15) Fanelli, F.; De Benedetti, P. G. *Chem. Rev.* **2005**, *105*, 3297−3351.
(16) Palczewski, K. *Annu. Rev. Biochem.* **2006**, *75*, 743−767.
(17) Gil, T.; Ipsen, J. H.; Mouritsen, O. G.; Sabra, M. C.; Sperotto, M. M.; Zuckermann, M. J. *Biochim. Biophys. Acta* **1998**, *1376*, 245−266.
(18) Jensen, M. Ø.; Mouritsen, O. G. *Biochim. Biophys. Acta* **2004**, *1666*, 205−226.
(19) Tieleman, D. P.; Forest, L. R.; Sansom, M. S.; Berendsen, H. J. *Biochemistry* **1998**, *37*, 17554−17561.
(20) Bond, P. J.; Sansom, M. S. P. *J. Am. Chem. Soc.* **2006**, *128*, 2697−2704.
(21) van Gunsteren, W. F.; et al. *Angew. Chem., Int. Ed.* **2006**, *45*, 4064−4092.
(22) Marrink, S. J.; de Vries, A. H.; Mark, A. E. *J. Phys. Chem. B* **2004**, *108*, 750−760.
(23) Shih, A. Y.; Arkhipov, A.; Freddolino, P. L.; Schulten, K. *J. Phys. Chem. B* **2006**, *110*, 3674−3684.
(24) Smeijers, A. F.; Pieterse, K.; Markvoort, A. J.; Hilbers, P. A. J. *J. Phys. Chem. B* **2006**, *110*, 13614−13623.
(25) Smit, B.; Hilbers, P. A. J.; Esselink, K.; Rupert, L. A. M.; Vanos, N. M.; Schlijper, A. G. *Nature* **1990**, *348*, 624−625.
(26) Ayton, G. S.; Voth, G. A. *J. Struct. Biol.* **2007**, *157*, 570−578.
(27) Marrink, S. J.; Mark, A. E. *Biophys. J.* **2004**, *87*, 3894−3900.
(28) Marrink, S. J.; Risselada, J.; Mark, A. E. *Chem. Phys. Lipids* **2005**, *135*, 223−244.
(29) Gabdoulline, R. R.; Wade, R. C. *Curr. Opin. Struct. Biol.* **2002**, *12*, 204−213.
(30) Grünberg, R.; Leckner, J.; Nilges, M. *Structure* **2004**, *12*, 2125−2136.
(31) Tang, C.; Iwahara, J.; Clore, G. M. *Nature* **2006**, *444*, 383−386.
(32) Okada, T.; Fujiyoshi, Y.; Silow, M.; Navarro, J.; Landau, E. M.; Shichida, Y. *Proc. Natl. Acad. Sci. U.S.A.* **2002**, *99*, 5982−5987.
(33) Mehler, E. L.; Periole, X.; Hassan, S. A.; Weinstein, H. *J. Comput.-Aided Mol. Des.* **2002**, *16*, 841−853.
(34) Berendsen, H. J. C.; Vanderspoel, D.; Vandrunen, R. *Comput. Phys. Commun.* **1995**, *91*, 43−56.
(35) Lindahl, E.; Hess, B.; van der Spoel, D. *J. Mol. Model.* **2001**, *7*, 306−317.
(36) van der Spoel, D.; Lindahl, E.; Hess, B.; Groenhof, G.; Mark, A. E.; Berendsen, H. J. C. *J. Comput. Chem.* **2005**, *26*, 1701−1718.
(37) Humphrey, W.; Dalke, A.; Schulten, K. *J. Mol. Graph.* **1996**, *14*, 33−8, 27−8.

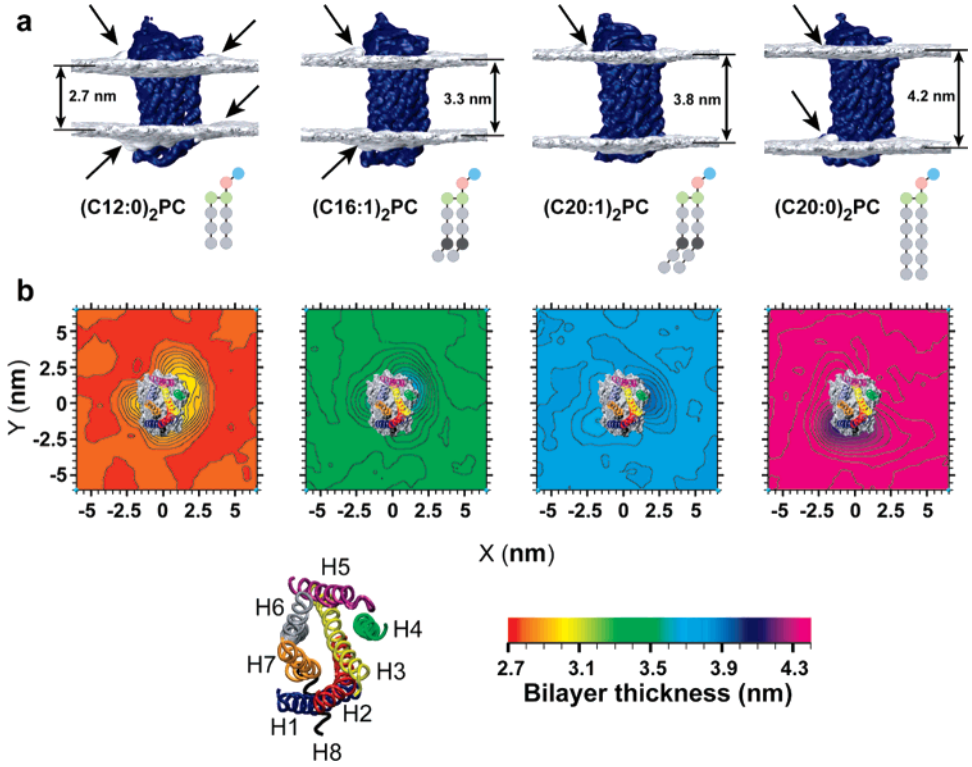

Figure 1. Membrane bilayers adapt to the presence of rhodopsin monomers. (a) Lateral views of time-averaged density profiles over entire simulations with the protein molecules centered and aligned before averaging. The Cα density of rhodopsin (dark blue) is shown with the extracellular and cytoplasmic domain toward the top and bottom, respectively. Phospholipid glycerol backbones of the bilayers are shown as isodensity surfaces (gray). Below each bilayer graphic are shown coarse-grain representations of the phospholipids: 1,2-didodecanoyl-*sn*-glycero-3-phosphocholine, $(C12:0)_2PC$; 1,2-di(10-*cis*-hexadecenoyl)-*sn*-glycero-3-phosphocholine, $(C16:1)_2PC$; 1,2-di(10-*cis*-eicosenoyl)-*sn*-glycero-3-phosphocholine, $(C20:1)_2PC$; and 1,2-dieicosanoyl-*sn*-glycero-3-phosphocholine, $(C20:0)_2PC$. Prominent membrane deformations (arrows) mostly consist of membrane thickening; inward deformities representing local thinning, as well as deformations due to protein tilt. (b) Topographic color contour maps showing the membrane thickness (red-orange to magenta) defined as in panel a by the distance glycerol density maxima of each monolayer. Rhodopsin is represented by its accessible surface (gray) and by the positions of individual protein helices, which are shown in color according to the schematic representation below. The data illustrate the localized bilayer perturbation by the presence of the protein. Hydrophobic mismatch results in curvature deformation and adaptation, especially pronounced in the case of the $(C12:0)_2PC$ bilayer (far left).

per unit cell at a protein-to-lipid ratio < 1:460) in a series of four phospholipid bilayers with different acyl chain lengths. The average membrane thicknesses, calculated from the density distributions of the glycerol backbones, ranged from 2.7 nm for $(C12:0)_2PC$ bilayers to 4.2 nm for $(C20:0)_2PC$ bilayers (Figure 1a). Differences in the average protein tilt and small protein conformational changes (Supporting Information, Figure 1) both contribute to slight differences in the average Cα density distributions of the protein in the different bilayers. The glycerol backbone densities are not homogeneous around the protein and differ for the two bilayer leaflets in the four model bilayers. This local sampling of the hydrophobic−hydrophilic boundary inscribed in the primary protein structure is consistent with earlier atomistic simulations.[38] Rhodopsin leads to alterations of the bilayer thicknesses at particular interfaces between the protein and the membrane (Figure 1b and Supporting Information Figure 2). Bilayer adaptation is reproducibly most pronounced as local thickening near helices H2, H4, and H7 in $(C12:0)_2PC$, $(C16:1)_2PC$, and $(C20:1)_2PC$ bilayers and as local thinning near helices H1/H8 and H5/H6 in $(C20:1)_2PC$ and $(C20:0)_2PC$. The persistence length of these thickness deformations is ∼1−2 nm, consistent with predictions from continuum models and atomistic simulations.[17,18] The localized effects revealed a non-uniform hydrophobic length of the TM domain of rhodopsin.

As a monomer, rhodopsin rotational (D_{rot}) and translational (D_{trans}) diffusion both decrease monotonically with the hydrophobic bilayer thickness of the membrane (Figure 2a). In the multi-copy simulations (16 rho), the diffusion coefficients start with values similar to those in the monomeric simulations (Figure 2a), but as the systems evolve, protein association leads to up to a 30-fold decrease of rhodopsin rotational mobility in the case of $(C12:0)_2PC$ and $(C16:1)_2PC$ bilayers. In contrast, the maximum change of the translational (lateral) mobility is only 5-fold, as seen in $(C12:0)_2PC$. This behavior is largely in agreement with the different functional dependency of translational and rotational diffusion coefficients on the bilayer thickness and the radius of the diffusing objects.[39−41] The mobility decreases with the bilayer thickness and the size of the diffusing object with a stronger effect on the rotational mobility. The increase of the effective radius of the diffusing object upon protein association and the effect on the measured rotational mobility[39] have been used to infer chain-length-dependent protein aggregation by electron paramagnetic reso-

(38) Huber, T.; Botelho, A. V.; Beyer, K.; Brown, M. F. *Biophys. J.* **2004**, *84*, 2078−2100.
(39) Saffman, P. G.; Delbrück, M. *Proc. Natl. Acad. Sci. U.S.A.* ***1975***, *72*, 3111−3113.
(40) Gambin, Y.; Lopez-Esparza, R.; Reffay, M.; Sierecki, E.; Gov, N. S.; Genest, M.; Hodges, R. S.; Urbach, W. *Proc. Natl. Acad. Sci. U.S.A.* **2006**, *103*, 2098−2102.
(41) Guigas, G.; Weiss, M. *Biophys. J* **2006**, *91*, 2393−2398.

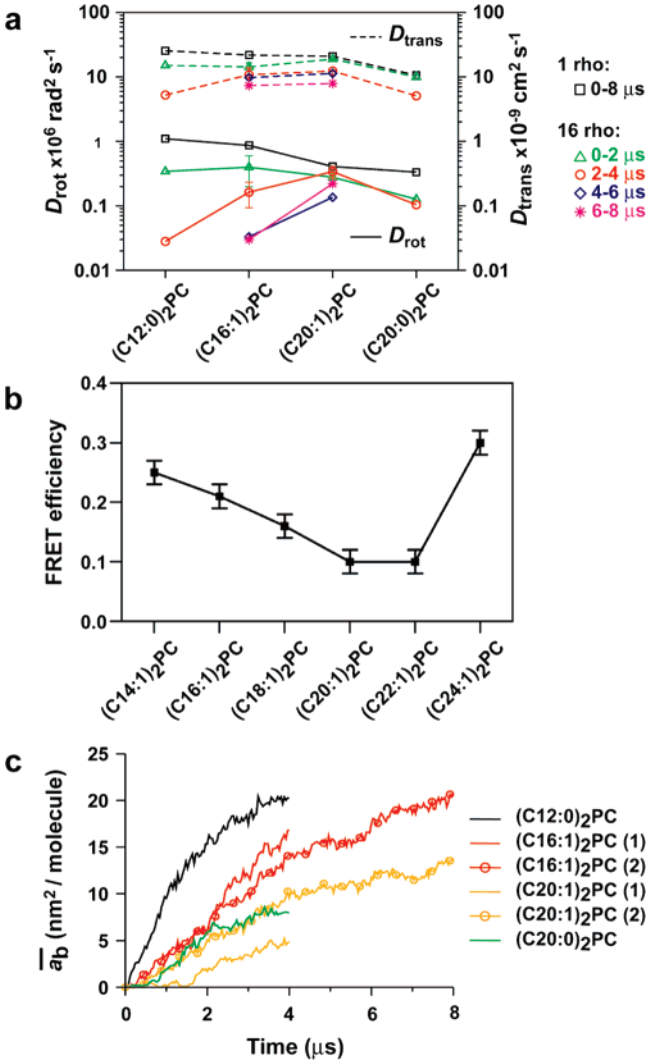

Figure 2. Membrane bilayer thickness affects rhodopsin self-assembly. (a) Protein rotational (D_{rot}) and translational (D_{trans}) diffusion coefficients are plotted for rhodopsin in (C12:0)$_2$PC, (C16:1)$_2$PC, (C20:1)$_2$PC, and (C20:0)$_2$PC bilayers with increasing thickness from left to right. The results for simulations using one rhodopsin (1 rho) and 16 rhodopsins (16 rho) per simulation cell can be compared for different time intervals, as shown. The dramatic reduction of rotational mobility in simulations with multiple rhodopsins in short-chain lipids is indicative of the formation of higher order protein structures. Rotational mobility (D_{rot}) is much more highly affected than translational mobility (D_{trans}) when rhodopsin self-assembles. (b) Fluorescence resonance energy transfer (FRET) was used to probe rhodopsin packing in membrane.[14] The FRET efficiency is plotted for a series of lipids (Cn:1)$_2$PC, with the acyl chain length n ranging from 14 to 24. The lower the transfer efficiency, the more distant are the probes and thus the more dispersed are rhodopsins. The optimal chain length for maximal dispersion is $n \approx 20-22$. Data for $n = 24$ may include a contribution from gel-state lipids. (c) The extent of protein association was quantitated by the buried ASA, a_b, averaged over *all* proteins (probe radius 0.26 nm) and plotted as a function of time, $\overline{a_b}(t)$, for each of the simulations listed. By definition $\overline{a_b}(0) = 0$ at the beginning of the simulation and increases over time as proteins associate in the bilayer to exclude intervening phospholipid molecules. The time-dependent increase in $\overline{a_b}(t)$ is correlated to bilayer thickness (see Figure 1a). Protein self-assembly is highest in thinner bilayers due to greater hydrophobic mismatch.

nance (EPR) experiments[11,13] and electron microscopy.[12,42] Accordingly, our simulations show the highest rotational mobility in the (C20:1)$_2$PC bilayer, which is slightly thicker than the (C16:0)$_2$PC found from the EPR experiments.[11] However, in the EPR studies, the different chain lengths were compared at different temperatures, complicating the interpretation as a purely hydrophobic mismatch effect. In order to clarify the situation, we studied rhodopsin packing in membranes as a function of bilayer thickness by fluorescence resonance energy transfer (FRET) experiments. The results for the homologous series of unsaturated lipids (Cn:1)$_2$PC (at 20 °C and ~1:100 protein-to-lipid ratio) gave clear evidence for non-random (non-ideal) dispersion of rhodopsin in membranes for bilayer thickness deviating from an optimal acyl chain length $n \approx 20-22$ (Figure 2b),[14] in good agreement with our simulations.

The evolution of protein contacts from the initially dispersed proteins in the membrane was analyzed as the buried accessible surface area (ASA) per protein, a_b. It reflects the surface area of the proteins involved in protein−protein contacts and thus not accessible to contact with water and membrane phospholipids. Averaged over all proteins and plotted as a function of time, $\overline{a_b}(t)$ shows how protein−protein contacts progressively exclude intervening phospholipid molecules (Figure 2c). A clear dependency on the lipid chain length can be appreciated. With increasing bilayer thickness in the series (C12:0)$_2$PC, (C16:1)$_2$PC, and (C20:1)$_2$PC, the kinetics of surface burial slows down progressively. However, in the thickest bilayer studied, (C20:0)$_2$PC, rhodopsin association again accelerates. Note that, in contrast to the pure bilayers,[22] we observed that rhodopsin inhibits gel-phase formation of this lipid. The time series of the radial correlation functions in the different phospholipid bilayers revealed a similar kinetics of the self-assembly process as a function of the bilayer thickness: it proceeds slowest in (C20:1)$_2$PC (Supporting Information Figure 3). The self-assembly process proceeds beyond dimers (see below), and it is not straightforward to assign simple rate and equilibrium constants. Consequently, we restrict ourselves to a qualitative description in the present development.

Visual inspection of snapshots of the (C16:1)$_2$PC and (C20:1)$_2$PC systems evolving over time (Figure 3a,c; Supporting Information, Movies 2 and 3) confirms the higher propensity for protein−protein contact interactions in (C16:1)$_2$PC. The probability histograms, $P(a_b)$, accumulated over 1-μs segments, show a rather narrow distribution close to zero within the first microsecond for both simulations (Figure 3b,d); rhodopsin monomers predominate initially. However, the formation of protein−protein contacts, reflected by the appearance of populations of proteins with increased a_b, is different in (C16:1)$_2$PC and (C20:1)$_2$PC. In (C16:1)$_2$PC, most monomers are recruited within 1−2 μs, and the system rapidly rearranges into growing clusters with a strong bias toward high a_b values. In (C20:1)$_2$PC, monomer recruitment primarily yields the formation of dimers within the first 4 μs (Figure 3c, central panel). Remarkable is the evolution of the histogram during the same period of simulation. There is a clear reorganization and increase of the dimer interfaces, indicating a search for shape complementarity that maximizes a_b. The reorganization of the interfaces is also visible from the snapshots of the system evolving in time (Figure 3a,c). During the last 4 μs, more monomers are recruited, resulting in proteins with more partners corresponding to the broad distribution of a_b values. The final snapshots show extended string-like clusters or organization in the (C16:1)$_2$PC system, whereas in (C20:1)$_2$PC bilayers, isolated aggregates are most abundant (Figure 3a,c).

(42) Chen, Y. S.; Hubbell, W. L. *Exp. Eye Res.* **1973**, *17*, 517−532.

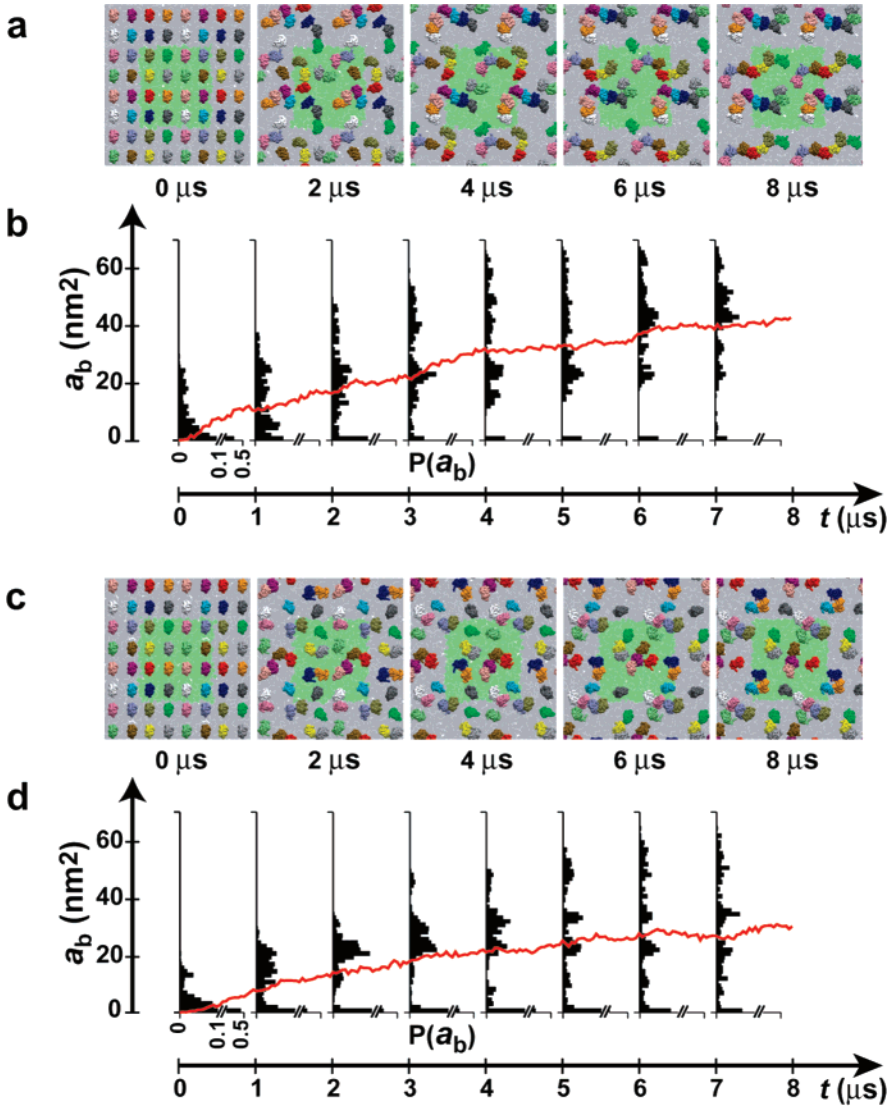

Figure 3. Spontaneous protein oligomerization in bilayers depends on hydrophobic mismatch. (a) Snapshots of instantaneous configurations of the proteins in the $(C16:1)_2PC$ bilayer at 0, 2, 4, 6, and 8 μs are shown from left to right. The central zone (green) indicates the simulation cell surrounded by periodic images (light gray). The proteins are uniquely color-coded. (b) The probability distribution histogram of the buried ASA, $P(a_b)$, for each individual protein (probe radius 0.52 nm) for a 1-μs segment of the 8-μs simulation in $(C16:1)_2PC$. The average of a_b over all molecules is shown as a function of time, $\overline{a_b}(t)$ (red line). (c) Snapshots of instantaneous configurations of the proteins in the $(C20:1)_2PC$ bilayer. (d) $P(a_b)$ in $(C20:1)_2PC$. Note that the distribution of a_b values for individual proteins in later segments varies more in the case of the $(C20:1)_2PC$ bilayer. This indicates that the proteins are less associated than those in the $(C16:1)_2PC$ bilayer.

To evaluate the structure of the protein assemblies formed during the simulations (Figure 4a), we constructed the in-plane projections of the Cα density of the TM helical segments around each monomer in the system (Figure 4b,c). On the 2−4-μs time scale, the projection maps (Figure 4b) show increasing protein Cα density around the reference protein in the series,

$$(C20:1)_2PC < (C20:0)_2PC < (C16:1)_2PC < (C12:0)_2PC$$

consistent with the hydrophobic-mismatch-driven process described above. This order is preserved at the 6−8-μs time scale, where available (Figure 4c). The maps indicate that, on a microsecond time scale, two-dimensional short-range order evolves in all systems, characteristic for a liquid-like condensed state of the proteins in the membrane plane, which is consistent with the fluid mosaic paradigm, including the feature of lipid-mediated protein−protein interactions.

Interestingly, the high and low Cα density regions in the first shell surrounding the central reference protein density exhibit some similarities in the different lipid environments, which suggests the existence of preferential protein−protein interaction sites in rhodopsin. The number of contact interfaces is clearly higher in $(C12:0)_2PC$ and $(C16:1)_2PC$, where strong forces are introduced by the hydrophobic mismatch, than in $(C20:1)_2PC$ and $(C20:0)_2PC$, where the forces are more in balance. Three contact zones are clearly visible on the 6−8-μs time scale in $(C20:1)_2PC$ (Figure 4c). They include previously suggested homo- and heterodimerization interfaces in rhodopsin and other GPCRs involving the exposed surfaces of the helices H1/H2/H8, H4/H5, and H6/H7, respectively (reviewed in ref 15). The projection maps and contact zones may be compared with the packing of frog rhodopsin in 2D crystals,[43] which maintains

(43) Schertler, G. F. X.; Hargrave, P. A. *Proc. Natl. Acad. Sci. U.S.A.* **1995**, *92*, 11578−11582.

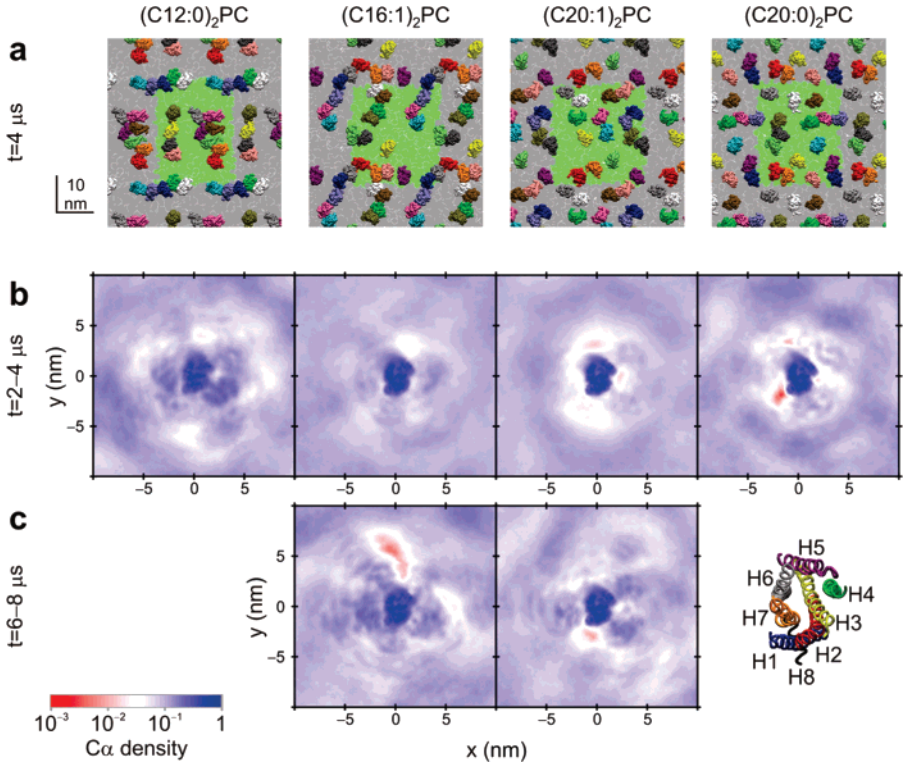

Figure 4. Hydrophobic mismatch drives self-assembly of receptors into liquid-like structures with short-range order. (a) Snapshots of instantaneous configuration of proteins in four different membrane environments at 4 μs. High-order aggregates are visible in $(C12:0)_2PC$ and $(C16:1)_2PC$, whereas mono-, di-, and trimers are predominant in $(C20:1)_2PC$ and $(C20:0)_2PC$. (b) Projection density maps show the lateral density profile of helical Cα atoms around a rhodopsin protein in a central reference position, with their helices oriented similar to the magnified scheme depicted in the lower right corner. The projection densities obtained from averages in the 2−4-μs range are shown for $(C12:0)_2PC$, $(C16:1)_2PC$, $(C20:1)_2PC$, and $(C20:0)_2PC$ bilayers. The data for $(C16:1)_2PC$ and $(C20:1)_2PC$ are averages of two independent simulations. The color scale (red to blue) denotes the Cα density of the TM helical segments. (c) The projection density maps obtained from averages of a single simulations in the 6−8-μs range are shown for $(C16:1)_2PC$ and $(C20:1)_2PC$ bilayers. The density maps (b,c) exhibit several local maxima in the direct vicinity of the central density, which corresponds to the reference protein, consistent with a liquid-like short-range order of the receptors.

the asymmetric protein orientation of the native membranes and exhibits receptor packing very similar to the model inferred from atomic force microscopy (AFM) studies of bovine rhodopsin in disc membranes.[4,44] It is striking to compare the locations of these interaction sites with the regions of the protein that drive the strongest response of the membrane to mismatch (Figure 1b), most pronounced for $(C12:0)_2PC$. The fact that they overlap indicates that lipid−protein and protein−protein interactions compete for the same interfaces (see below).

Discussion

In general, protein−protein complex formation can be described as a multi-stage process. The initial step of diffusional association leads to the diffusional encounter complex, and subsequent non-diffusional rearrangement yields the fully bound complex.[29−31] For fast-associating protein pairs, the diffusional association process is determined by long-range forces, such as electrostatic interactions, which enable translational and orientational steering of proteins toward an aligned diffusional encounter complex that influences the kinetics of protein−protein association.[29] Rearrangement of the encounter complex to the fully bound complex involves desolvation of the protein interfaces, and recognition of matching conformations on the basis of shape complementarity is a key controlling factor.[30]

How do the data presented here relate to a mechanism of rhodopsin self-assembly in membranes? The adaptation of the phospholipids to the non-uniform shape of the polar and hydrophobic interfaces of the protein results in local deformation of the bilayer from its equilibrium thickness (Figure 1b). This can be assimilated to medium- and long-range attractive forces between proteins.[17] The simulations with multiple rhodopsins, starting from a (non-equilibrium) well-separated initial configuration, allow us to follow the kinetics of the early relaxation toward equilibrium for rather small ensembles of molecules. Apparently, strong deformations of the bilayer (Figure 1b) are correlated with increased rates of protein association, measured by $\overline{a_b}(t)$ (Figure 2c). In the absence of strong deformation, the diffusional encounter appears biased toward non-random sites (Figure 3b,d, Figure 4b,c; Supporting Information Figure 4). Moreover, non-uniform shape limits possible arrangements with reasonable surface complementarity (Figure 4b,c) that would maximize a_b (Figure 3b,d). The results are consistent with the notions that local distortion of the bilayer is likely to influence protein interactions and that, for example, the peripheral energy of distorting the bilayer may enhance interactions that reduce the peripheral contour length.[3] Furthermore, it has been shown that elastic deformations of a bilayer, due to either positive or negative hydrophobic mismatch, both result in attractive protein−protein interactions, but for negative mismatch the attractions is less pronounced and an additional energetic barrier appears.[45]

(44) Liang, Y.; Fotiadis, D.; Filipek, S.; Saperstein, D. A.; Palczewski, K.; Engel, A. *J. Biol. Chem.* **2003**, *278*, 21655−21662.

Our observation of low-occupancy regions surrounding the central protein in the case of $(C20:0)_2PC$, and to a smaller extent in the case of $(C20:1)_2PC$ (Figure 4b,c), might reflect such energetic barriers due to localized negative mismatch. In addition, shell-like structure of solvating lipids results in energetic barriers for the desolvation process upon protein contact formation,[46] and in analogy to the hydrophobic effect, it has been suggested that lipid entropy may be an important driving force for membrane protein complex formation.[47] We propose that, in membranes, lipid-mediated protein−protein interactions provide an additional mechanism that governs the association process[29] by long-range forces and possibly intermediate-range repulsive barriers.

With respect to the oligomeric state of rhodopsin, early biophysical experiments described rhodopsin as a mobile monomer in the rod−cell disc membrane,[48,49] in line with the classical view of a freely diffusing particle in a fluid membrane.[1] Recently, AFM images showed rhodopsins arranged in rows of dimers,[4] 25−50 nm long, tightly packed together—a static distribution that would appear to conflict with a freely diffusing rhodopsin.[50] In agreement with earlier experimental reports,[11−14] our simulations show that rhodopsin does tend to oligomerize and that the membrane environment affects the extent of oligomerization. In addition, we observed a liquid-like order of the protein in the membrane with a site preference for protein−protein contacts. Therefore, our view of rhodopsin self-assembly in membranes is consistent with the "mosaic" aspect of the fluid mosaic model,[3] where short-range order (patches) is predicted. The original fluid mosaic model, proposed more than three decades ago, already suggested the possibility of "short-range order" in the membrane, even though order was thought to be absent over distances of "a few tenths of a micrometer and greater".[1] In the ongoing debate regarding the functional and physiological relevance of 7-TM receptor oligomerization, especially in Type 1 GPCRs,[4−7,15,16,51] these findings present a future challenge for both experimental and theoretical approaches,[8] because true dimerization will have to be discriminated from transient random protein−protein contacts,[7] as well as from hydrophobic-mismatch-driven protein−protein contacts.

In conclusion, we addressed the problem of membrane protein solvation by lipid bilayers. In particular, we investigated the effect of hydrophobic mismatch between the bilayer and protein on protein oligomerization. We chose a model system, the GPCR rhodopsin, in which self-assembly or self-organization, as opposed to ligand-induced association or assembly during biosynthesis, predominates, although the functional consequence of rhodopsin dimerization has been controversial. CGMD simulations of single and multi-copy rhodopsin in four different mismatch conditions were performed. In summary, translational and rotational protein mobility, protein buried ASA, protein−protein radial correlation functions, and projected Cα densities all describe qualitatively the same behavior of self-assembly kinetics with bilayer thickness: the presence of hydrophobic mismatch favors rhodopsin aggregation. Moreover, protein−protein interactions inside a membrane bilayer show a site preference related to localized mismatch. Any model system has intrinsic limitations, and accurate descriptions of complex biological systems are difficult.[21] However, careful parametrization and a dramatically expanded time scale and size dimension of the simulated membrane system have allowed us to identify novel principles relevant to understanding receptor assembly in complex biological membranes. We anticipate that future application of the CGMD method will contribute to a better understanding of the role of lipid diversity[8] and protein structure[3] in lipid-mediated protein−protein interactions. The detailed, yet static, view on models of complex biological membranes, such as synaptic vesicles,[52] may be enhanced by our method by addition of the fourth dimension—time.

Acknowledgment. The work was supported by Ellison Medical Foundation (T.P.S.) and the Allene Reuss Memorial Trust (T.P.S.). The use of the Dutch national supercomputing facilities (SARA) is gratefully acknowledged.

Supporting Information Available: Three movies illustrating typical CGMD trajectories for some systems; detailed description of the forces fields and models used here, additional analysis plots (Supporting Information Figures 1−4), and complete refs 21 and 52. This material is available free of charge via the Internet at http://pubs.acs.org.

JA0706246

(45) Bohinc, K.; Kralj-Iglič, V.; May, S. *J. Chem. Phys.* **2003**, *119*, 7435−7444.
(46) Lagüe, P.; Zuckermann, M. J.; Roux, B. *Biophys. J* **2000**, *79*, 2867−2879.
(47) Helms, V. *EMBO Rep.* **2002**, *3*, 1133−1138.
(48) Cone, R. A. *Nat.—New Biol.* **1972**, *236*, 39−43.
(49) Liebman, P. A.; Entine, G. *Science* **1974**, *185*, 457−459.
(50) Chabre, M.; Cone, R.; Saibil, H. *Nature* **2003**, *426*, 30−31.
(51) Chabre, M.; le Maire, M. *Biochemistry* **2005**, *44*, 9395−9403.
(52) Takamori, S.; et al. *Cell* **2006**, *127*, 831−846.